



# Numerical simulation of the fluid flow and heat transfer of the supercritical water in the 64-element Canadian SCWR fuel bundle

Huirui Han & Chao Zhang

**To cite this article:** Huirui Han & Chao Zhang (2023) Numerical simulation of the fluid flow and heat transfer of the supercritical water in the 64-element Canadian SCWR fuel bundle, *Journal of Nuclear Science and Technology*, 60:10, 1228-1243, DOI: [10.1080/00223131.2023.2188269](https://doi.org/10.1080/00223131.2023.2188269)

**To link to this article:** <https://doi.org/10.1080/00223131.2023.2188269>



Published online: 21 Mar 2023.



Submit your article to this journal 



Article views: 147



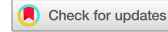
View related articles 



View Crossmark data 



ARTICLE



# Numerical simulation of the fluid flow and heat transfer of the supercritical water in the 64-element Canadian SCWR fuel bundle

Huirui Han and Chao Zhang

Department of Mechanical & Materials Engineering, Western University, London, ON Canada

## ABSTRACT

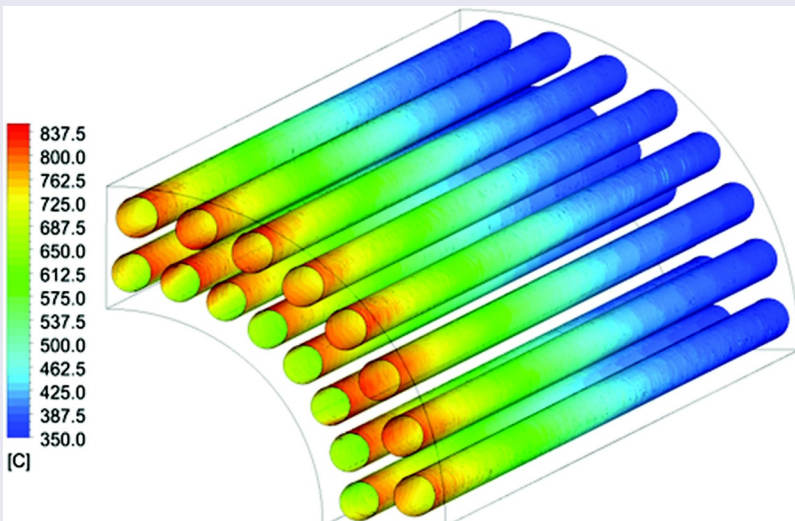
Canada has participated in the Generation IV nuclear energy systems focusing on the Supercritical Water-cooled Reactor (SCWR) system. The 64-element fuel rods channel is used in the Canadian SCWR. There are few publicly available experimental studies for the flow in the fuel channels with multiple fuel rods. To date, the CFD simulation reported in open literature for rod bundle flow in the 64-element SCWR is relatively scarce. The cladding surface temperature is of key importance in assessing the safety of the reactor. Since the inhomogeneities in the bundle cross-section can present complex flow phenomena, a CFD study can provide substantial insight into the flow physics. In this work, the full-scale CFD simulation of the supercritical water flow in the 64-element rod bundle was performed. The results suggest the possibility of the presence of gap vortices in the flow subchannels. Higher streamwise velocities and normal Reynolds stresses always exist at the center subchannel regions. The circumferential cladding surface temperature distribution is extremely non-uniform and there is a large difference between the maximum cladding surface temperatures for different fuel rods.

## ARTICLE HISTORY

Received 7 June 2022  
Accepted 13 February 2023

## KEYWORDS

Supercritical Water-cooled Reactor (SCWR); CFD; rod bundle; cladding surface temperature



## 1. Introduction

Supercritical Water-Cooled Reactors (SCWRs) were proposed as one of the six Generation IV nuclear reactors [1]. The Canadian SCWR core concept is based on the pressure tube reactor design. With the supercritical steam at a pressure between 23.5 MPa and 38 MPa and the turbine inlet temperature of 540–625°C, the thermal efficiency can be up to 55% [2]. The coolant in the SCWR is a once-through direct cycle, i.e. the superheated steam exiting the reactor flows to the turbine directly. Consequently, steam generators and separators are not needed, which results in

a reduced capital cost and lower maintenance cost because of fewer components. However, before the reactor is put into construction, it is important to predict the temperature distribution in the reactor to make sure the proposed reactor can operate safely under the design condition. During the past few years, several researchers have conducted experimental studies on the supercritical water flows in the circular tubes [3–10]. The heat transfer mechanism varies with operating conditions and there is no common consensus on the experimental results for the criteria of the heat transfer deterioration. Recently,

limited experimental studies were conducted for the supercritical water flow in a channel with fuel rods [11–13]. The experimental data for the supercritical water flows in the fuel rod channels in the open literature are quite limited. Due to the cost of the experiments and technical difficulties to obtain more detailed velocity and heat transfer data inside the rod bundle experimentally, the computational fluid dynamics (CFD) method has been used for investigating and understanding the fluid flow and heat transfer phenomenon in the supercritical water channels for many years [14–18].

Several approaches can be used to solve the conservation equations which govern the flow field in the CFD simulations, including the direct numerical simulations (DNS), the large eddy simulations (LES), and the Reynolds-averaged Navier–Stokes simulation (RANS). Since the DNS needs to solve all flow motion scales, the applicability of the DNS is restricted to relatively small geometries due to the high computational cost. Thus, DNS is not commonly used in the study for nuclear reactors. Some researchers conducted the LES simulations for nuclear reactors. Fischer et al. [19] performed the LES simulations on a single fuel pin through the spectral method. Merzari et al. [20] and Brockmeyer et al. [21] consecutively using Nek500 code to simulate the flow in a 7-pin reactor geometry. Brockmeyer et al. [22] applied STARCCM+ software to perform the LES in a 19-pin flow geometry with a shortened rod length. Recently, Goth et al. [23] employed the same code to investigate the flow behaviors in a 61-pin geometry. Although the LES is more applicable than the DNS in the study of nuclear reactors. There are still some limitations. The Reynolds number should be less than around 20,000 for large flow geometries [24]. In practical applications, the Reynolds number of the flow in the reactor usually exceeds this number. Thus, the RANS method is widely used in the numerical study of the high turbulent supercritical water flow in nuclear reactors. Several turbulent models can be used in the simulation of supercritical fluid flows. Jones and Launder [25] first proposed the standard  $k-\epsilon$  turbulence model for the condition of the fully developed turbulent flows where the influence of the molecular viscosity is not considered. To be applicable in a wider class of flows than the standard model, the renormalization group theory (RNG)  $k-\epsilon$  model using a mathematical technique was developed [26]. Subsequently, the realizable  $k-\epsilon$  model was developed [27], which differs from the standard one in satisfying certain mathematical constraints on the Reynolds stress in order to be consistent with the physics of the turbulent flow. It shows better performance for the flows involving rotation

and the boundary layers under strong adverse pressure gradients. Wilcox [27] presented the standard  $k-\omega$  model. This model shows an improved performance for the boundary layer under strong adverse pressure gradients. Later, the  $k-\omega$  shear stress transport (SST) model was proposed by Menter [28]. The modification is that the linear constitutive equation of the standard  $k-\omega$  allows the  $k-\omega$  model used in the boundary layer region while the  $k-\epsilon$  model used for the free stream region. Kim et al. [29] investigated the vertical upward supercritical water flow in a heated tube by selected turbulent models: standard, RNG, and realizable  $k-\epsilon$  models, standard  $k-\omega$  and  $k-\omega$  SST models. The numerical results were compared with the experimental data from Yamagata et al. [10]. Although the RNG  $k-\epsilon$  model with the enhanced wall treatment showed the best performance, the predictions of the wall temperatures are not satisfactory. The above two-equation turbulent models are based on the assumption of the isotropic eddy-viscosity. The Reynolds stress model (RSM) closes the Reynolds-averaged Navier–Stokes equations by solving transport equations for the Reynolds stresses directly and together with an equation for the dissipation rate without the isotropic hypothesis.

The numerical studies by RANS simulations for the supercritical flow in rod bundles have been investigated by several researchers recently. Zhao et al. [30] used OpenFOAM to simulate a 7-pin flow geometry with the  $k-\omega$  SST turbulence model for different operation conditions. Zhang et al. [31] simulated the heat transfer and flow of the supercritical water in a 37-element horizontal arranged SCWR under steady state condition and found that the anisotropic turbulent model, the Reynolds stress model, behaves much better than the isotropic model in predicting the cladding surface temperature. Furthermore, Han et al. [32] further applied the same turbulence model for the simulation in the vertical channel with multiple fuel rods. Similar investigations can also be found in [33,34]. The heat transfer characteristics in different type channels were investigated. A recent validation study of the RANS models for different fuel rod assemblies was performed by Dovizio et al. [35]. It was found that the RANS could be a reasonable approach to study this kind of fuel assemblies.

Differing from the current pressurized heavy water reactors, the proposed Canadian SCWR adopted a vertical fuel channel and the coolant is light water at a supercritical condition. The length of the fuel assembly of the Canadian SCWR is 5 m, which is much longer than that used in the pressurized heavy water reactor. So, the aspect ratio of the fuel bundle in the Canadian SCWR is much larger than those in the preceding reactors. There is no experimental data for the Canadian SCWR

available and there is still lack of a full-scale investigation on the fluid flow and heat transfer phenomenon for the supercritical water in the 64-element fuel bundle. In this work, the supercritical water flow in the proposed Canadian SCWR with 64-element fuel bundle is investigated numerically by the RANS approach and the detailed fluid flow and heat transfer phenomenon for the supercritical water flow in the fuel rod channels are presented. The CFD simulations are carried out by the commercial software ANSYS FLUENT.

## 2. Numerical procedure

### 2.1. Configurations and operating conditions of the Canadian SCWR

The Canadian SCWR core is proposed as shown in Figure 1. There are 336 fuel channels in the Canadian SCWR core and generate a total 2540 MW thermal power. The operating pressure is 25 MPa. In the fuel assembly, the coolant flows downward through a central flow tube, and then flows upward through the fuel rod bundle region. The

fuel bundle consists of 64-element two-ring fuel rods. For each ring, 32 fuel elements are distributed circumferentially around the insulated central flow tube. The cross-section view of the fuel bundle is presented schematically in Figure 2. The operating conditions of the Canadian SCWR are shown in Table 1 [36].

### 2.2. Computational domain

In this study, only a quarter of the region with fuel rods in the fuel bundle is considered in the numerical simulation because of the symmetry to reduce the computational time. The computational domain and the types of flow subchannels are shown in Figure 3. The symmetry planes are indicated in Figure 3(a). Figures 3(b-c) illustrate two types of subchannels in the flow channel: the inner central subchannels between fuel rods and the edge subchannels between fuel rods and the edges of the fuel bundle. The geometry specifications and operating conditions of the 64-element Canadian SCWR are shown Table 1 [36]. The thermal physical

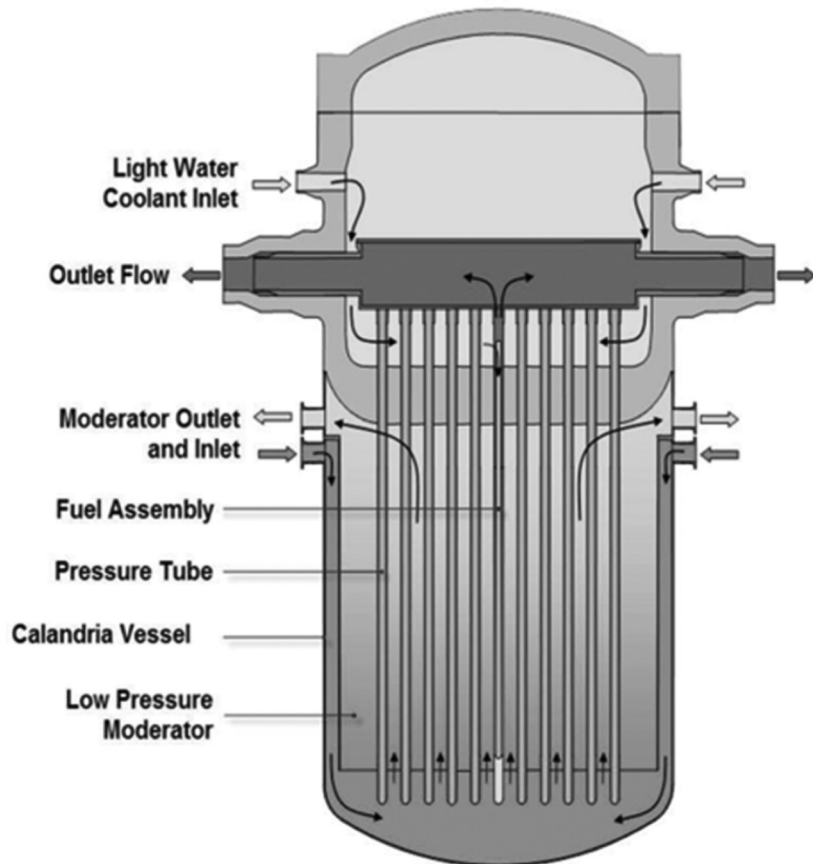
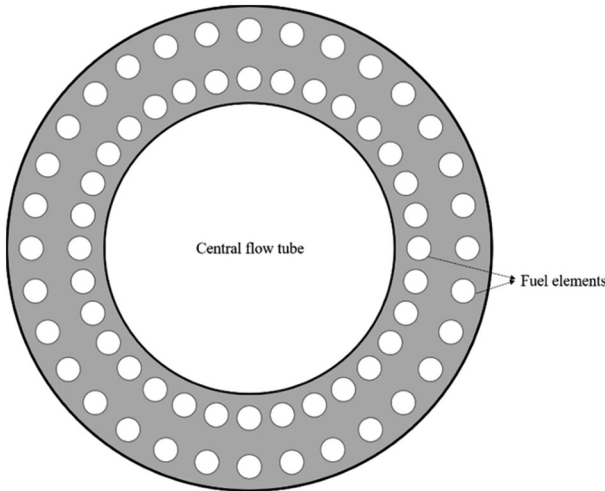
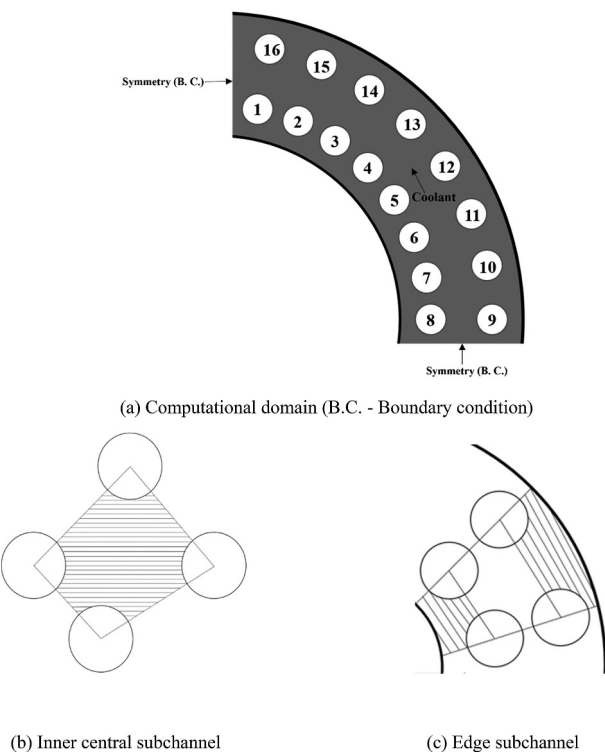


Figure 1. Canadian SCWR core concept [36].



**Figure 2.** Cross-section view of the 64-element fuel assembly.



**Figure 3.** Computational domain and subchannel types.

**Table 1.** Geometry specifications of the fuel bundle and operating conditions of the 64-element Canadian SCWR [36].

Inner/Outer fuel rod diameter	9.5/10 mm
Inner/Outer tube radius	46/72 mm
Heated length	5 m
Operating pressure	25 MPa
Coolant mass flow rate in the fuel bundle	3.93 kg/s
Coolant inlet temperature	350°C
Coolant inlet density	625 kg/m <sup>3</sup>
Thermal Power	2540 MW
Cladding temperature limit	850°C

properties of the supercritical water were calculated by the physical property software (National Institute of Standards and Technology, NIST) and added to the ANSYS fluent using piecewise linear fitting method.

### 2.3. Numerical model and governing equations

The governing equations for this three-dimensional steady state flow and heat transfer are conservations of mass, momentum, and energy, which are shown in the Reynolds averaged form as follows [37]:

$$\frac{\partial \rho \bar{u}_i}{\partial x_i} = 0 \quad (1)$$

$$\frac{\partial (\rho \bar{u}_i \bar{u}_j)}{\partial x_j} = -\frac{\partial \bar{p}}{\partial x_i} + \frac{\partial}{\partial x_j} \left( \mu \frac{\partial \bar{u}_i}{\partial x_j} - \rho \bar{u}'_i \bar{u}'_j \right) + \rho g_i \quad (2)$$

$$\frac{\partial}{\partial x_i} (\bar{u}_i \rho c_p T) = \frac{\partial}{\partial x_i} \left[ \left( \lambda + \frac{c_p \mu_t}{Pr_t} \right) \frac{\partial T}{\partial x_i} \right] + \phi \quad (3)$$

The modified Reynolds stress model with the variable  $Pr_t$  for supercritical fluid flows proposed in a previous study [38] is used in the simulations of the supercritical water flow in the 64-element fuel bundle. The Reynolds stresses,  $-\rho \bar{u}'_i \bar{u}'_j$ , are solved by the Reynolds stress model to close the momentum equation. The transport equations for the Reynolds stress model can be described as:

$$\begin{aligned} \frac{\partial}{\partial x_k} (\rho u_k \bar{u}'_i \bar{u}'_j) &= \underbrace{-\frac{\partial}{\partial x_k} \left[ \rho \bar{u}'_i \bar{u}'_j u'_k + p' (\delta_{kj} u'_i + \delta_{ik} u'_j) \right]}_{C_{ij} = \text{Convection}} \\ &\quad + \underbrace{\frac{\partial}{\partial x_k} \left[ \mu \frac{\partial}{\partial x_k} (\bar{u}'_i \bar{u}'_j) \right]}_{D_{L, ij} = \text{Molecular Diffusion}} - \rho \left( \bar{u}'_i \bar{u}'_k \frac{\partial u_j}{\partial x_k} + \bar{u}'_j \bar{u}'_k \frac{\partial u_i}{\partial x_k} \right) - \rho \beta \left( g_i \bar{u}'_j \theta + g_j \bar{u}'_i \theta \right) \\ &\quad + \underbrace{p' \left( \frac{\partial u'_i}{\partial x_j} + \frac{\partial u'_j}{\partial x_i} \right)}_{\phi_{ij} = \text{Pressure Strain}} - 2\mu \underbrace{\frac{\partial \bar{u}'_i}{\partial x_k} \frac{\partial \bar{u}'_j}{\partial x_k}}_{\epsilon_{ij} = \text{Dissipation}} - 2\rho \Omega_k \left( \bar{u}'_j \bar{u}'_m \epsilon_{ikm} + \bar{u}'_i \bar{u}'_m \epsilon_{jkm} \right) \\ &\quad + \underbrace{S_{user}}_{User-Defined Source Term} \end{aligned} \quad (4)$$

Because of the drastic changes of the thermal physical properties of the supercritical water, the turbulent

Prandtl number is not a constant value [38,39], which is modeled as a piecewise function:

$$Pr_t = \begin{cases} 0.4 & \mu_t/\mu < 0.2 \\ 0.3 + 0.03 * \frac{P}{P_{cr}} * P_r * (\mu_t/\mu) * (q/G) & 0.2 \leq \mu_t/\mu \leq 10 \\ 0.85 & \mu_t/\mu > 10 \end{cases} \quad (5)$$

The enhanced wall treatment is selected for the near wall treatment with the RSM and the mesh is fine enough to ensure  $y^+ \approx 1$  near the wall. The example of the near wall mesh is shown in Figure 4. The enhanced wall treatment modeling method uses a blended wall function, which blends the separate models in the two-layer approach using a damping function to have a smoother transition between the two. The boundary conditions are set based on the operating conditions given in Table 1. The reference pressure is 25 MPa. The inlet velocity is 1.05 m/s based on the mass flow rate of the coolant and the inlet temperature is 350°C, respectively. The heat flux on the fuel rod is assumed uniform at 880 kW/m<sup>2</sup>, which is calculated based on the thermal power of 2540 MW. All rod surfaces are set as no-slip boundary condition. Both the central tube wall and the outer edge have the adiabatic boundary conditions. A mesh sensitivity study is conducted. The simulations using three different meshes with increasing the number of cells are executed. Table 2 presents the characteristics of the meshes and the comparison of the respective simulation results. The outlet velocity magnitude is defined as the magnitude of the velocity vector at the outlet. It can be seen that the relative differences of the simulations results are small and decreases with the mesh becoming finer. Considering the accuracy of the simulation results and the cost of the computation, mesh 2 is employed in this simulation to investigate the flow physics in the rod channel. ANSYS Fluent software is used in this study to perform the computational fluid dynamics simulations.

## 3. Results and discussions

### 3.1. Velocity and temperature profiles

The streamwise velocity profile in the cross-section at the outlet is provided in Figure 5(a), which demonstrates the primary feature of the flow field. It is found that the distribution of the streamwise velocity component is similar along the circumferential direction and the streamwise velocities at the inner central subchannels are higher than those at edge subchannels. Therefore, the coolant temperatures at the inner central subchannels are higher than those at the edge subchannels as shown in Figure 5(b).

Figure 6 displays 6 lines (Lines 1 to 6) along the radial direction, which are used for quantitative

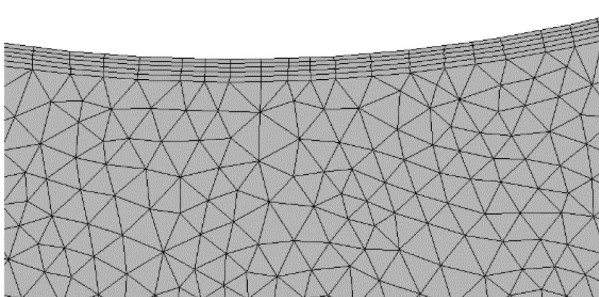
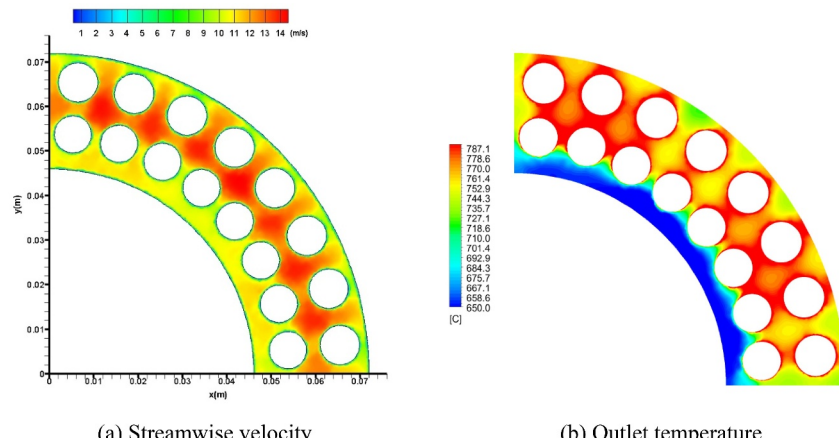


Figure 4. Central subchannel and edge subchannel.

**Table 2.** Mesh characteristics and the comparison results.

Mesh ID	Cells	Maximum wall temperature (°C) at z = 5 m	Rod where the maximum wall temperature exists	Relative difference between consecutive meshes (%)	Outlet velocity magnitude (m/s)	Relative difference between consecutive meshes (%)
1	6139234	828.3	Rod # 15		12.05	
2	11419161	836.9	Rod # 15	1.04	11.67	3.15
3	19578137	838.5	Rod # 15	0.19	11.73	0.51



**Figure 5.** Distributions of the streamwise velocity (m/s) and outlet temperature (°C) at the outlet.

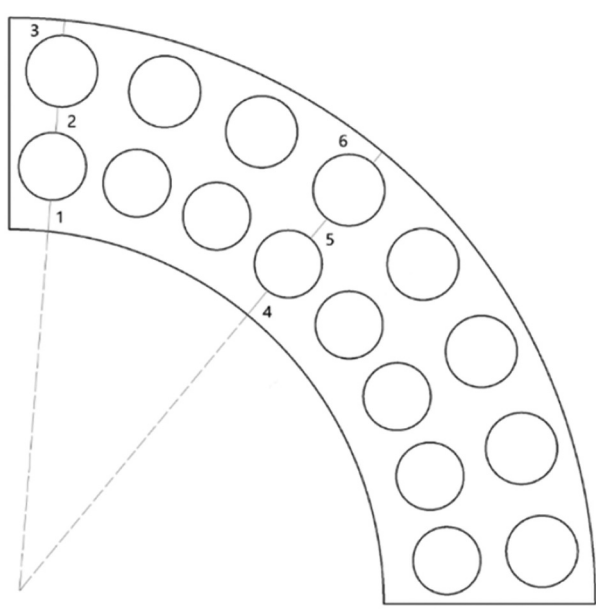


**Figure 6.** Lines used for analysis.

comparisons in subsequent plots. These lines span the gaps between the inner wall and rod, between the rods, and between the rod and outer wall from the inner wall to the outer wall. The radial distribution of the streamwise velocity profiles along these six lines are provided in Figure 7. As

expected, the velocities are higher in the region away from the walls and decrease sharply toward the near wall region. And the gradient of the velocity decrease along the radial direction at edge subchannels (lines 1, 3, 4, 6) are smaller than those at central subchannels (lines 2, 5).

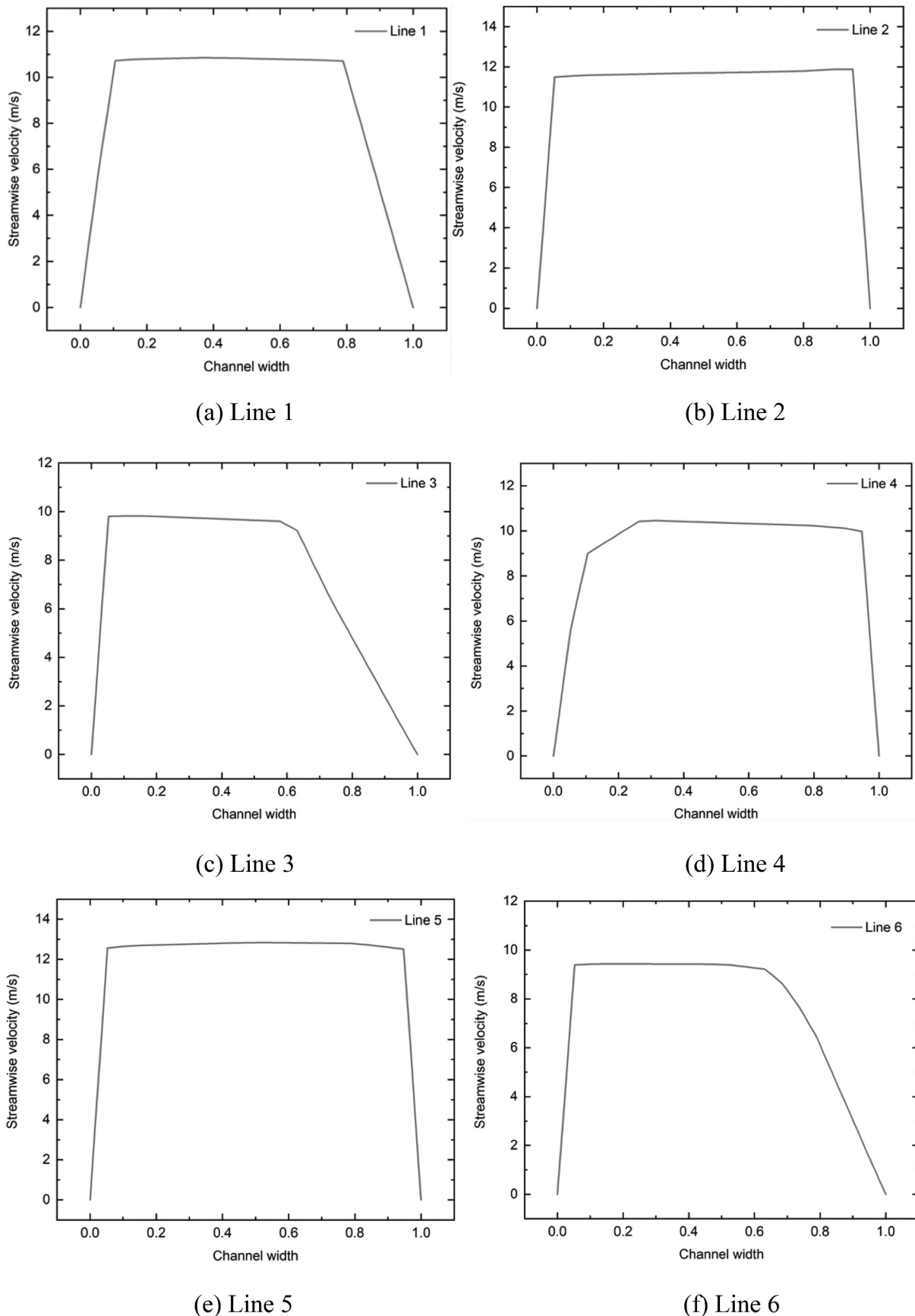


**Figure 7.** Plots of the streamwise velocity along lines (m/s).

Based on studies by Jones and Launder [25] and Orszag et al. [26], the re-laminarization of the flow occurs when the velocity profiles of fluid flow show 'flatten' shape with weakened turbulent kinetic energy in the boundary layer. This would result in heat transfer deterioration.

### 3.2. Reynolds stresses and turbulent kinetic energy

Reynolds stresses and turbulent kinetic energy were also extracted from the CFD results. Figure 8 provides the distributions of the normal

Reynolds stresses in three different directions and turbulent kinetic energy at the outlet. It can be seen from the figure that as expected in wall-bounded shear flows, the streamwise Reynolds stress ( $w'w'$ ) is higher than the other two components throughout most of the domain. Generally, the turbulent kinetic energy in central subchannels is higher than that at edge subchannels, which is similar to the streamwise Reynolds stress distribution. The normal Reynolds stresses along each line are provided in Figures 9–10. In these figures, the channel width is the normalized. The streamwise Reynolds is up to 6 times higher than the other

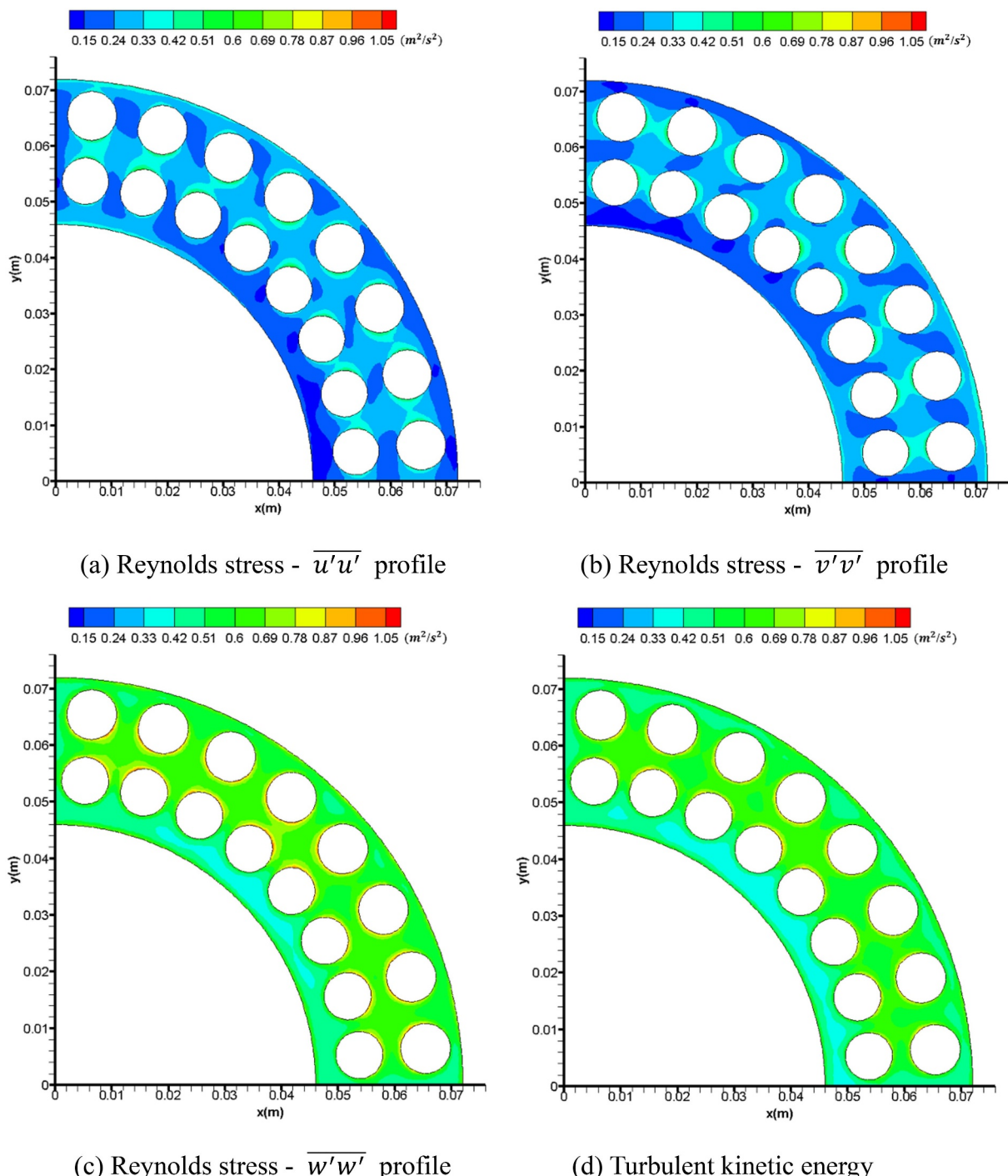
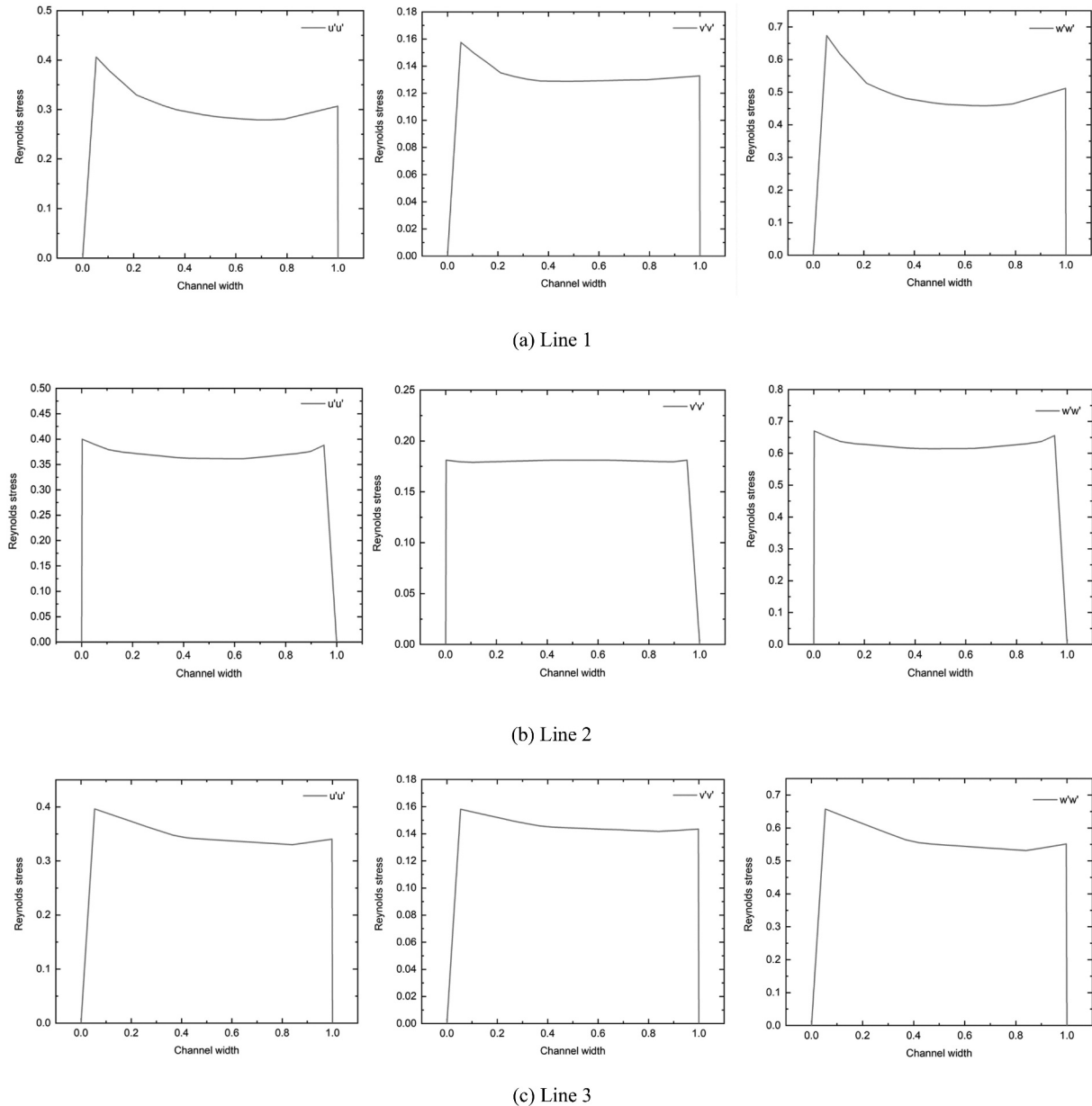


Figure 8. Distributions of the normal Reynolds stresses and turbulent kinetic energy at the outlet ( $m^2/s^2$ ).



**Figure 9.** Plots of Reynolds normal stresses for lines 1–3 ( $m^2/s^2$ ).

two components. It shows that the streamwise Reynolds stress has dual peaks between channel walls of all subchannels, and the peak values are larger in the edge subchannels than those in the central subchannels. The lateral stresses follow a similar pattern but with reduced peaks due to less production from the mean shear. With the dramatic increase in the normal Reynolds stresses and the turbulent kinetic energy from the wall to the free stream, the heat transfer from the wall to the free stream could be enhanced.

### 3.3. Secondary flow

The lateral secondary flows in rod bundles are important for inter-channel mixing and heat transfer. With the assumption of the symmetric

flow domain, the results of the simulation still confirm that there are non-organized lateral motions in the flow at the outlet, presented in Figure 11. The cross flows show that in the edge subchannel, such as near Rod #1, the flow is moving towards the rod, whereas in the center subchannel, such as near Rod #7, the flow is moving toward the center of the subchannel. It can be seen vortices are formed in the regions near Rods #1 and #7, which supports further evidence of the existence of gap vortex in the subchannels [40,41]. The gap vortex is defined as strong transverse motions across the narrow gaps between neighboring fuel elements or between a fuel element and the containing vessel wall. The gap vortex could enhance dramatically the mixing between flows in adjacent subchannels. It should

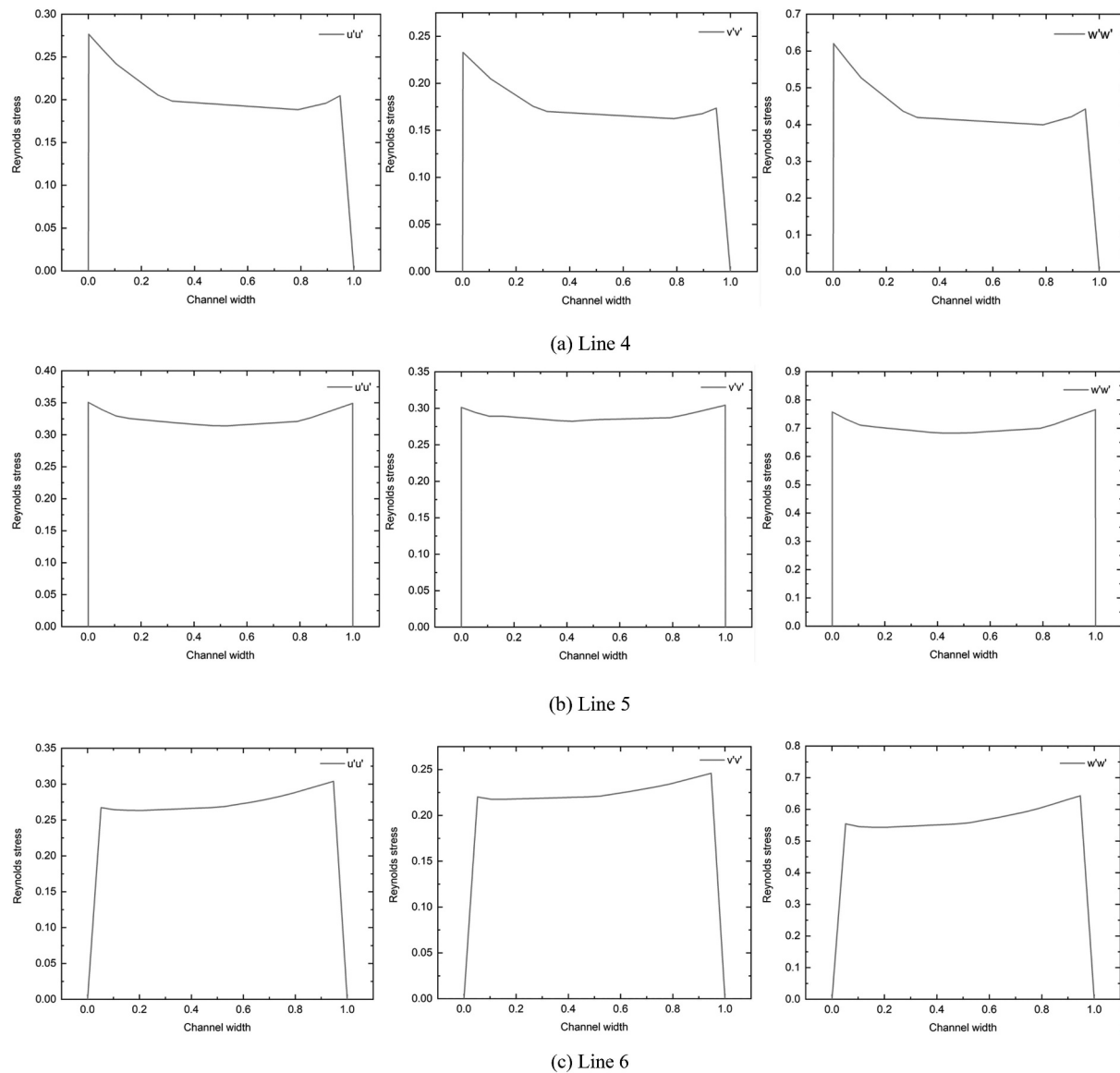


**Figure 10.** Plots of Reynolds normal stresses for lines 4–6 ( $m^2/s^2$ ).

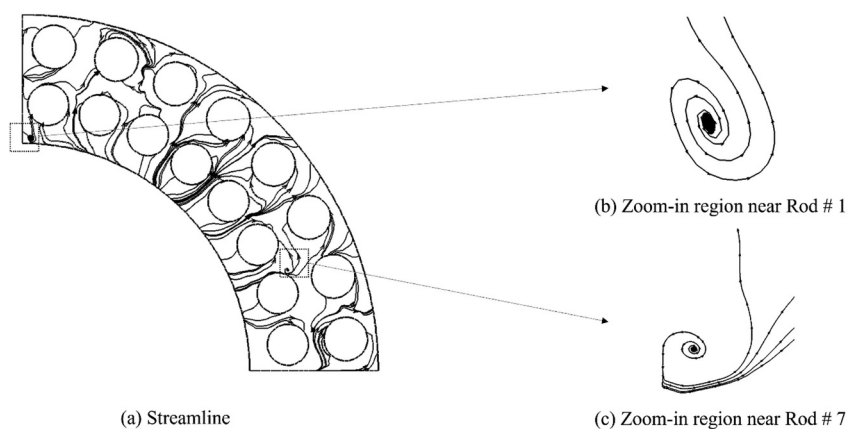


**Figure 11.** Streamline of the cross flow at the outlet.

be noted that the vortex in the region near Rod #1 could result from the symmetric treatment of the plane near Rod #1 and such vortex is not observed in other edge subchannels.

### 3.4. Bulk temperature & wall temperature

The bulk temperature of the supercritical water, which is the mass-weighted average fluid temperature, and the specific heat at the cross section along the axial direction are shown in Figure 12. The fluid temperature increases along the upward flow direction from 350°C at the inlet to about 741°C at the exit. The specific heat has the maximum value at around  $z = 1$  m, which is near the pseudocritical point ( $T_{pc} = 384.9^\circ\text{C}$ ). This implies that the heat absorption here is stronger than at other temperatures. However, the thermal conductivity and density also fall quickly around the

pseudocritical point. The significant density variation results in the intensive buoyancy effect, which would consequently suppress the turbulent diffusion and impair heat transfer. Figure 13 depicts the circumferential distribution of the cladding surface temperatures on the fuel rods in the entire domain. It can be seen that the cladding temperature increases in along the axial direction. But the maximum cladding surface temperature, which is around 837°C, in the reactor at the design point is below the upper limit of 850°C. This means that the proposed Canadian SCWR can be operated safely under the design operating condition.

The maximum and minimum cladding surface temperatures along the circumference of the fuel rods at  $z = 2.5$  m,  $z = 3.75$  m, and  $z = 5$  m are also shown in Figures 14–16. The bulk fluid temperatures at these three planes are 448.4°C, 573.9°C, and 741°C, respectively. It is found that the

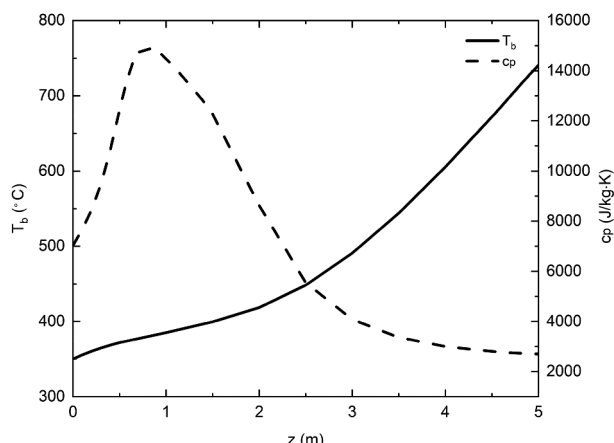


Figure 12. Bulk temperature and specific heat distributions along the axial direction.

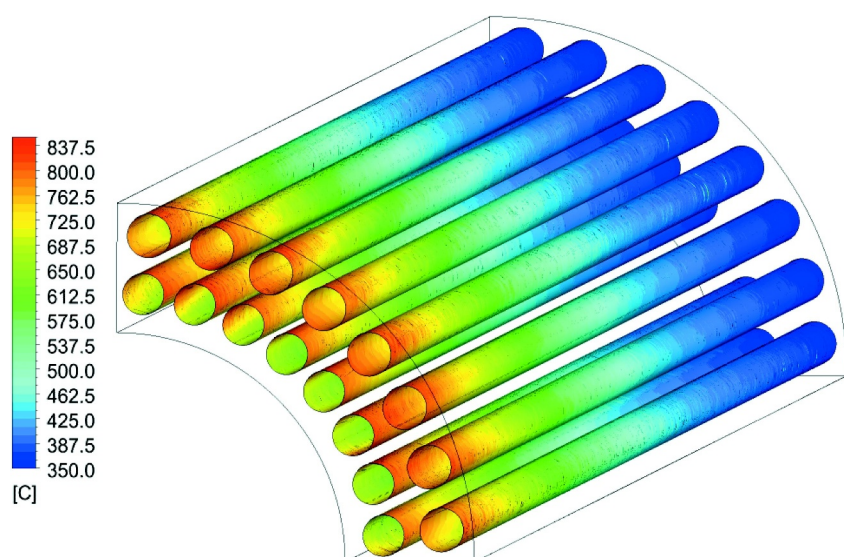
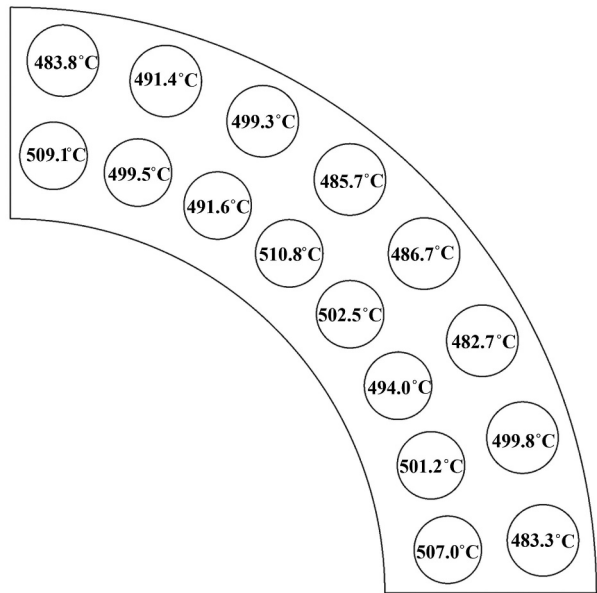
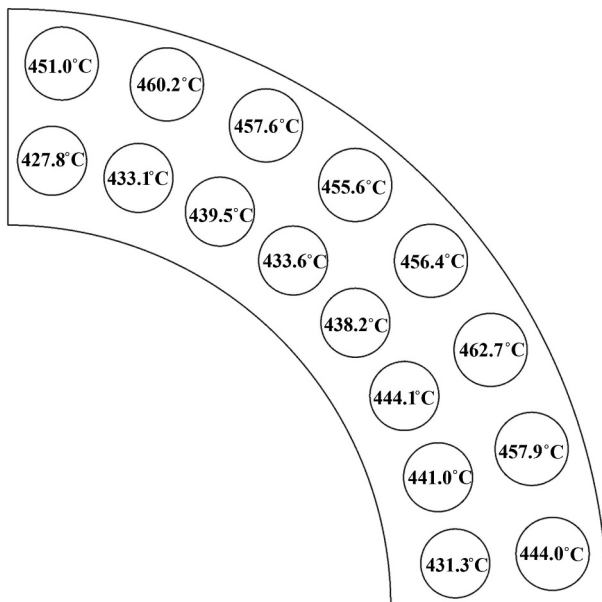


Figure 13. Cladding surface temperature distributions in the fuel bundle.



(a) Maximum

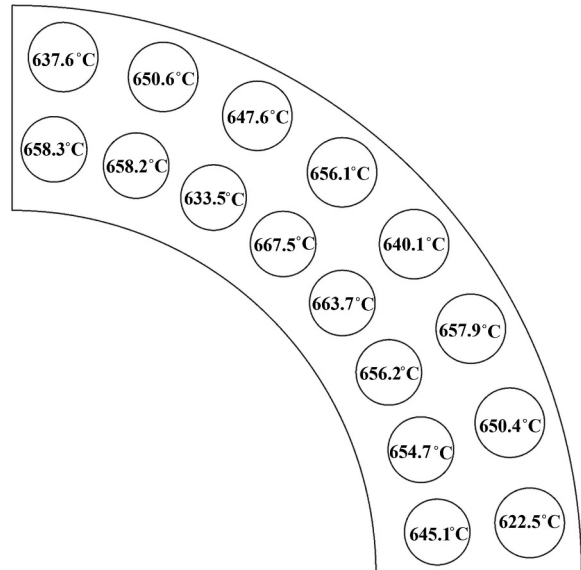


(b) Minimum

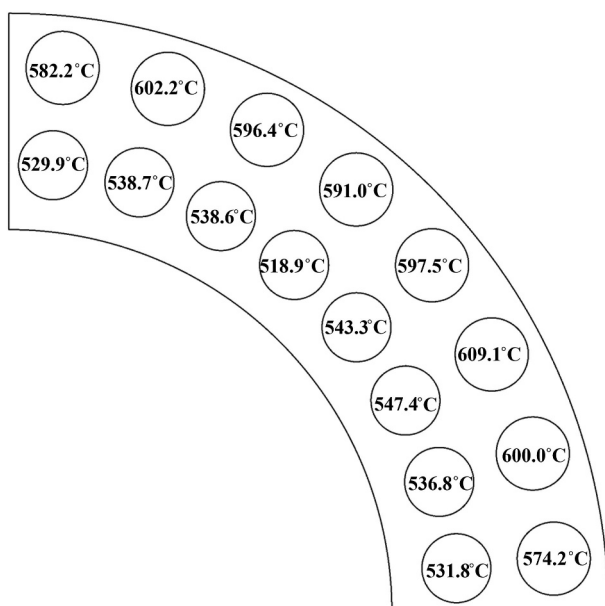
**Figure 14.** Maximum and minimum cladding surface temperatures along the circumference of the fuel rods at  $z = 2.5$  m ( $^{\circ}\text{C}$ ).

maximum cladding surface temperatures at  $z = 2.5$  m,  $z = 3.75$  m, and  $z = 5$  m occur at Rods #4, #4 and #15, respectively, while the minimum cladding surface temperatures appear at fuel Rods #1, #4, and #4, respectively. The results show that the largest circumferential cladding surface temperature difference is  $182.2^{\circ}\text{C}$  at  $z = 5$  m of fuel Rod #4.

The axial cladding surface temperature distributions at the Rods #2, #4 and #15 along  $z = 2.5$  m – 5 m are shown in Figure 17. Figure 17(a) indicates



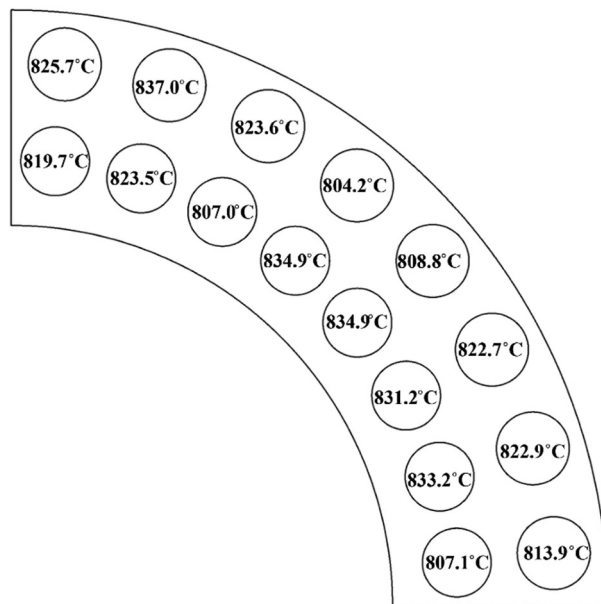
(a) Maximum



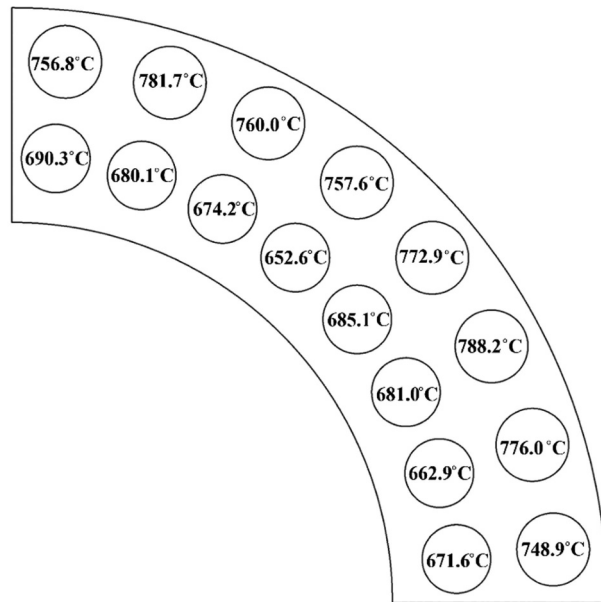
(b) Minimum

**Figure 15.** Maximum and minimum cladding surface temperatures along the circumference of the fuel rods at  $z = 3.75$  m ( $^{\circ}\text{C}$ ).

the definition of angles used in this figure. It can be seen that for Rod #2 and Rod #4, which are the inner layer rods, the temperature is lower at  $0^{\circ}$ , which is in the region close to the inner wall in the fuel bundle, while the temperatures at  $90^{\circ}$ ,  $180^{\circ}$  and  $270^{\circ}$  are similar and higher than that at  $0^{\circ}$ . The axial cladding surface temperature distribution at  $0^{\circ}$ ,  $90^{\circ}$ ,  $180^{\circ}$ , and  $270^{\circ}$  at Rod #15, which is an outer layer rod, are similar. Figure 18 presents the cladding surface temperature distribution



(a) Maximum



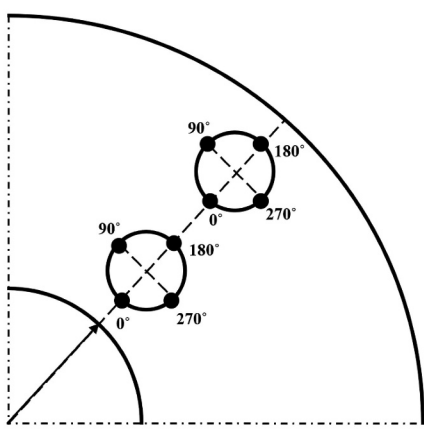
(b) Minimum

**Figure 16.** Maximum and minimum cladding surface temperatures along the circumference of the fuel rods at z = 5 m (°c).

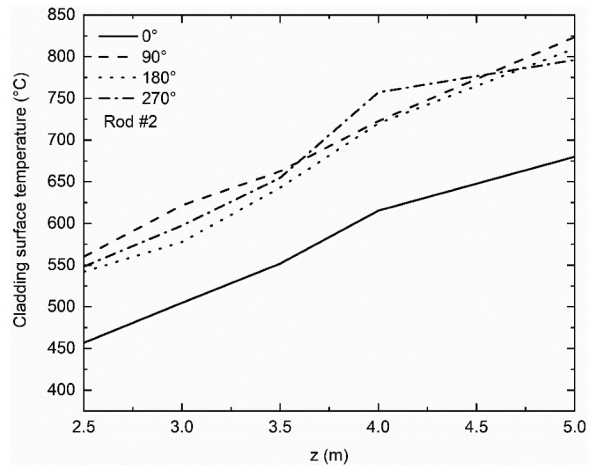
along the circumference for fuel Rod #4 at z = 5 m. It can be concluded that the wall temperature is higher at the inner central subchannel region, which is 90° to 270° for the inner layer rods, than that at the edge subchannel region, which is at 0°. Although the maximum cladding surface temperature is below limit of 850°C, the maximum wall temperature for each fuel rod is quite different and the temperature of the circumferential direction is very non-uniform.

#### 4. Conclusion

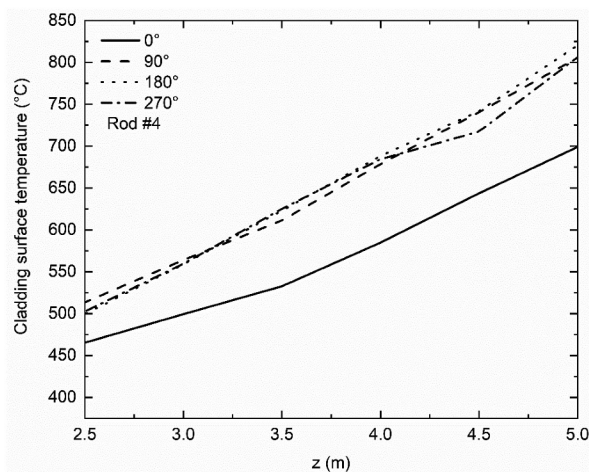
In this study, CFD studies were performed using turbulent model with a modified turbulent Prandtl number to simulate the full-scale 3D flow and heat transfer of the supercritical water in the bundles with fuel rods for the first time. The CFD results indicated that maximum temperature of the proposed Canadian SCWR under the design conditions is the below the limit for the safe operation of the system. The fluid flow and heat transfer phenomena in the



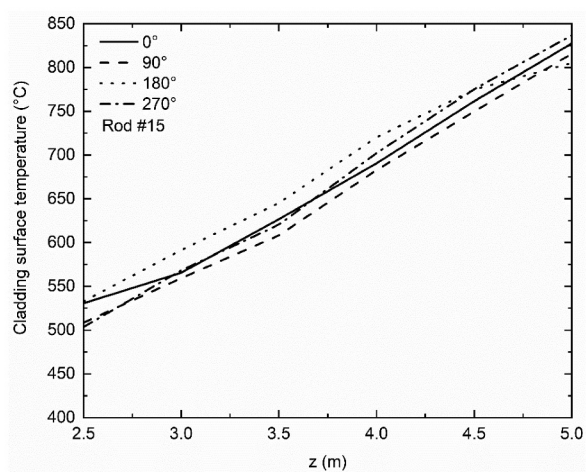
(a) Definition of the angles used in the figure



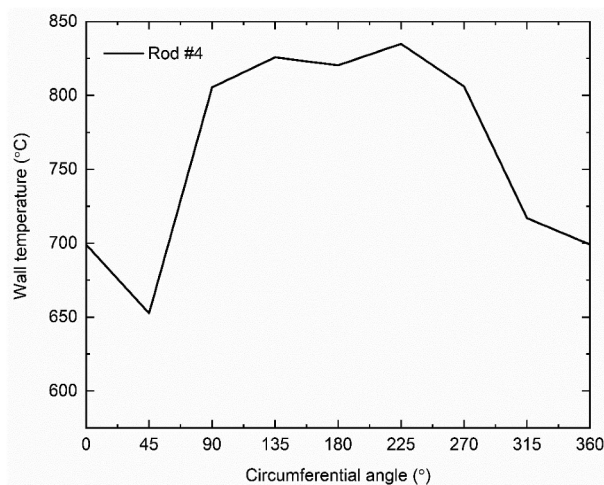
(b) Rod # 2



(c) Rod # 4



(d) Rod # 15

**Figure 17.** Axial cladding surface temperature distributions along different rods.**Figure 18.** Circumferential cladding surface temperature distribution at  $z = 5$  m for Rod #4.

rod bundle have been clarified, especially the possibility of the existence of the gap vortex in the edge subchannels. This phenomenon might be due to the intrinsic aspects of

the turbulence and geometry of the flow subchannels, which are similar to the previous studies for the rod bundle flow. The fluid bulk temperature and the wall temperatures

of the fuel rods generally increase along the axial flow direction. It is observed that the circumferential wall temperature distribution around the fuel rod surface is extremely non-uniform and the maximum cladding surface temperature for each fuel rod is also different. Higher wall temperatures exist at inner central subchannel regions with surrounding four heating rods. The maximum cladding temperature and the circumferential distributions are significant for the safety design of the assembly of the nuclear reactor, notably when there are accidental disturbances. Thus, a more appropriate thermal power distribution for each fuel rod based on the present work is needed. In addition, the respective experimental work is needed in the future to validate the numerical results.

## Nomenclature

### Symbols

$c_p$	Specific heat, J/kg·K
$g$	Gravitational acceleration, m/s <sup>2</sup>
$k$	Turbulence kinetic energy, m <sup>2</sup> /s <sup>2</sup>
$P$	Pressure, Pa
$\text{Pr}$	Prandtl number
$T$	Temperature, °C
$u$	Velocity, m/s
$y^+$	Nondimensional distance from the wall, $y^+ = \frac{u_t y}{v}$ ( $y$ : distance from the wall, m)
$z$	Axial location, m

### Greek letters

$\varepsilon$	Turbulence kinetic energy dissipation, m <sup>2</sup> /s <sup>3</sup>
$\mu$	Dynamic viscosity, Pa · s
$\lambda$	Thermal conductivity, W/m · K
$\rho$	Density of a fluid, kg/m <sup>3</sup>
$\delta_{ij}$	Kronecker delta tensor, $\delta_{ij} = 1$ if $i = j$ , $\delta_{ij} = 0$ if $i \neq j$
$\omega$	Specific dissipation rate, 1/s

### Subscripts

$cr$	Critical
$t$	Turbulent

### Acronyms

3D	Three-dimensional
CFD	Computational Fluid Dynamics
DNS	Direct Numerical Simulation
RNG	Renormalization Group
RSM	Reynold Stress Model
SCWR	Supercritical Water-Cooled Reactor
SST	Shear Stress Transport
LES	Large Eddy Simulation
RANS	Reynolds-Averaged Navier-Stokes simulation
RSM	Reynolds Stress Model

### Disclosure statement

No potential conflict of interest was reported by the authors.

## Funding

This work was supported by the Natural Sciences and Engineering Research Council of Canada (NSERC) Discovery grant [grant number #04757]

## ORCID

Huirui Han  <http://orcid.org/0000-0001-9475-6957>

## References

- [1] GIF(Generation IV International Forum). R&D outlook for generation IV nuclear energy systems 2018 update. **2018**.
- [2] Pioro I, Duffey RB, Kirillov PL et al. Pros and cons of commercial reactor designs part 1: current status of electricity generation in the world and selected countries. In E. B. T.-E. of N. E. Greenspan, Ed. Encyclopedia of nuclear energy: Elsevier. **2021**. pp. 263–287.
- [3] Qu M, Yang D, Liang Z et al. Experimental and numerical investigation on heat transfer of ultra-supercritical water in vertical upward tube under uniform and non-uniform heating. International Journal of Heat & Mass Transfer. **2018** Dec;127:769–783.
- [4] Lei X, Li H, Dinh N et al. A study of heat transfer scaling of supercritical pressure water in horizontal tubes. International Journal of Heat & Mass Transfer. **2017**;114:923–933.
- [5] Shen Z, Yang D, Wang S et al. Experimental and numerical analysis of heat transfer to water at supercritical pressures. International Journal of Heat & Mass Transfer. **2017**;108:1676–1688.
- [6] Gu HY, Zhao M, Cheng X. Experimental studies on heat transfer to supercritical water in circular tubes at high heat fluxes. Exp Therm Fluid Sci. **2015**;65:22–32.
- [7] Yu S, Li H, Lei X et al. Experimental investigation on heat transfer characteristics of supercritical pressure water in a horizontal tube. Exp Therm Fluid Sci. **2013** Oct;50:213–221.
- [8] Zhang G, Zhang H, Gu H et al. Experimental and numerical investigation of turbulent convective heat transfer deterioration of supercritical water in vertical tube. Nucl Eng Des. **2012** Jul;248:226–237.
- [9] Mokry SJ, Kirillov PL, Pioro IL et al. Supercritical water heat transfer in a vertical bare tube: normal, improved, and deteriorated regimes. Nucl Technol. **2010**;172(1):60–70.
- [10] Yamagata K, Nishikawa K, Hasegawa S et al. Forced convective heat transfer to supercritical water flowing in tubes. International Journal of Heat & Mass Transfer. **1972**;15(12):2575–2593.
- [11] Wang H, Bi Q, Wang L et al. Experimental investigation of heat transfer from a  $2 \times 2$  rod bundle to supercritical pressure water. Nucl Eng Des. **2014** Aug;275:205–218. DOI:[10.1016/J.NUCENGDES.2014.04.036](https://doi.org/10.1016/J.NUCENGDES.2014.04.036).
- [12] Gu HY, Li HB, Hu ZX et al. Heat transfer to supercritical water in a  $2 \times 2$  rod bundle. Ann Nucl Energy. **2015**;83:114–124.
- [13] Zhao M, Gu HY. Experimental and numerical investigation on heat transfer of supercritical water flowing

- upward in  $2 \times 2$  rod bundles. *Nucl Eng Des.* **2020**;370 (October):110903.
- [14] Zhang B, Shan J, Jiang J. Numerical analysis of supercritical water heat transfer in horizontal circular tube. *Prog Nucl Energy.* **2010**;52(7):678–684.
- [15] Xiong J, Cheng X. Turbulence modelling for supercritical pressure heat transfer in upward tube flow. *Nucl Eng Des.* **2014** Apr;270:249–258.
- [16] Zhang B, Shan JQ, Jiang J. Simulation of heat transfer of supercritical water in obstacle-bearing vertical tube. *Nuclear Science and Techniques.* **2010**;21 (4):241–245.
- [17] Wen QL, Gu HY. Numerical simulation of heat transfer deterioration phenomenon in supercritical water through vertical tube. *Ann Nucl Energy.* **2010**;37 (10):1272–1280.
- [18] Zhang Y, Zhang C, Jiang J. Numerical simulation of heat transfer of supercritical fluids in circular tubes using different turbulence models. *J Nucl Sci Technol.* **2011**;48(3):366–373.
- [19] Fischer P, Lottes J, Siegel A et al., Large eddy simulation of wire-wrapped fuel pins i: hydrodynamics in a periodic array. in Joint International Topical Meeting on Mathematics & Computation and Supercomputing in Nuclear Applications, Monterey, CA, USA, **2007**.
- [20] Merzari E, Fischer P, Yuan H et al. Benchmark exercise for fluid flow simulations in a liquid metal fast reactor fuel assembly. *Nucl Eng Des.* **2016** Mar;298:218–228. DOI:[10.1016/J.NUCENGDES.2015.11.002](https://doi.org/10.1016/J.NUCENGDES.2015.11.002).
- [21] Brockmeyer L, Merzari E, Solberg J et al. One-way coupled simulation of FIV in a 7-pin wire-wrapped fuel pin bundle. *Nucl Eng Des.* **2020** Jan;356:110367. DOI:[10.1016/J.NUCENGDES.2019.110367](https://doi.org/10.1016/J.NUCENGDES.2019.110367).
- [22] Brockmeyer L, Carasik LB, Merzari E et al. Numerical simulations for determination of minimum representative bundle size in wire wrapped tube bundles. *Nucl Eng Des.* **2017** Oct;322:577–590. DOI:[10.1016/j.nucengdes.2017.06.038](https://doi.org/10.1016/j.nucengdes.2017.06.038).
- [23] Goth N, Jones P, Nguyen DT et al. Comparison of experimental and simulation results on interior subchannels of a 61-pin wire-wrapped hexagonal fuel bundle. *Nucl Eng Des.* **2018** Nov;338:130–136. DOI:[10.1016/j.nucengdes.2018.08.002](https://doi.org/10.1016/j.nucengdes.2018.08.002).
- [24] Bovati O, Yildiz MA, Hassan Y et al. RANS simulations for transition and turbulent flow regimes in wire-wrapped rod bundles. *Int J Heat Fluid Flow.* **2021** Aug;90(June):108838.
- [25] Jones WP, Launder BE. The prediction of laminarization with a two-equation model of turbulence. *Int J Heat Mass Transf.* **1972**;15(2):301–314.
- [26] Orszag S, Yakhot V, Flannery W et al. Renormalization group modeling and turbulence simulations. *Int. Conf. Near-Wall Turbul. Flows.* **1993**;1031–1046.
- [27] Wilcox DC. Turbulence modeling for CFD, vol. 2: DCW industries La; **1998**.
- [28] Menter FR. Two-equation eddy-viscosity turbulence models for engineering applications. *Aiaa J.* **1994**;32 (8):1598–1605.
- [29] Kim SH, Kim YI, Bae YY et al. Numerical simulation of the vertical upward flow of water in a heated tube at supercritical pressure. *Proc. 2004 Int. Congr. Adv. Nucl. Power Plants, ICAPP'04.* **2004**;1527–1534.
- [30] Zhao P, Liu J, Ge Z et al. CFD analysis of transverse flow in a wire-wrapped hexagonal seven-pin bundle. *Nucl Eng Des.* **2017** Jun;317:146–157. DOI:[10.1016/J.NUCENGDES.2017.03.038](https://doi.org/10.1016/J.NUCENGDES.2017.03.038).
- [31] Zhang Y, Zhang C, Jiang J. Numerical simulation of fluid flow and heat transfer of supercritical fluids in fuel bundles. *J Nucl Sci Technol.* **2011**;48 (6):929–935.
- [32] Han H, Zhang C. Numerical simulation of fluid flow and heat transfer of the supercritical water in different fuel rod channels. **2018**. DOI:[10.25071/10315/35367](https://doi.org/10.25071/10315/35367).
- [33] Yang X, Su GH, Tian W et al. Numerical study on flow and heat transfer characteristics in the rod bundle channels under super critical pressure condition. *Ann Nucl Energy.* **2010**;37(12):1723–1734.
- [34] Podila K, Rao Y. CFD modelling of supercritical water flow and heat transfer in a  $2 \times 2$  fuel rod bundle. *Nucl Eng Des.* **2016** May;301:279–289.
- [35] Dovizio D, Mikuž B, Shams A et al. Validating RANS to predict the flow behavior in wire-wrapped fuel assemblies. *Nucl Eng Des.* **2020** Jan;356:110376. DOI:[10.1016/J.NUCENGDES.2019.110376](https://doi.org/10.1016/J.NUCENGDES.2019.110376).
- [36] Yetisir M, Hamilton H, Xu R et al. Fuel assembly concept of the canadian supercritical water-cooled reactor. *J Nucl Eng Radiat Sci.* **2018**;4(1):1–7.
- [37] ANSYS. Inc. 14.0 ANSYS FLUENT theory guide. **2011**.
- [38] Han H, Zhang C. A modified turbulent model for the supercritical water flows in the vertical upward channels. *J Supercrit Fluids.* **2022** Aug;187:105632. DOI:[10.1016/j.supflu.2022.105632](https://doi.org/10.1016/j.supflu.2022.105632).
- [39] Kong X, Sun D, Gou L et al. Numerical investigation on heat transfer of supercritical water with a variable turbulent prandtl number model. *J Nucl Eng Radiat Sci.* **2020**;6(3):1–10.
- [40] Tavoularis S. Rod bundle vortex networks, gap vortex streets, and gap instability: a nomenclature and some comments on available methodologies. *Nucl Eng Des.* **2011** Jul;241(7):2624–2626. DOI:[10.1016/j.nucengdes.2011.03.052](https://doi.org/10.1016/j.nucengdes.2011.03.052).
- [41] Merzari E, Ninokata H. Anisotropic turbulence and coherent structures in eccentric annular channels. *Flow Turbul Combust.* **2009**;82(1):93–120.